(15) Vrentas, J. S.; Duda, J. L.; Ni, L.-W. *Macromolecules* **1983**, *16*, 261.
(16) Huston, E. L.; Cahn, J. W.; Hilliard, J. E. *Acta Metall.* **1966**, *14*, 1053.
(17) Flory, P. J. *J. Chem. Phys.* **1942**, *10*, 51.
(18) Tompa, H. "Polymer Solutions"; Butterworths: London, 1956.
(19) Caneba, G. T.; Soong, D. S. *Macromolecules*, in press.
(20) Scott, R. L. *J. Chem. Phys.* **1945**, *13*, 178.
(21) Koningsveld, R.; Stockmayer, W. H.; Kennedy, J. W.; Kleintjens, L. A. *Macromolecules* **1974**, *7*, 73.

Polymer Membrane Formation through the Thermal-Inversion Process. 2. Mathematical Modeling of Membrane Structure Formation

Gerard T. Caneba* and David S. Soong

Department of Chemical Engineering, University of California, Berkeley, California 94720.
Received April 11, 1985

ABSTRACT: Formation of anisotropic membranes by thermal inversion is simulated by a model developed here. Structured membranes are formed when a polymer/solvent film is thermally coagulated from one face while the opposite face is thermally insulated. Both kinetics and thermodynamics of liquid–liquid phase separation are included in the analysis. Only noncrystalline polymers are considered, and the composition of the starting polymer solution is close to the critical or Θ composition of the polymer/solvent system. Hence, spinodal decomposition is taken as the mechanism of phase separation. For a given point in the membrane cross section, the degree of phase separation is characterized by the deviation of the fluctuating concentration profile from the concentration of the starting polymer solution. The use of the Flory–Huggins model for solution thermodynamics and Cahn–Hilliard theory for spinodal decomposition leads to a one-dimensional fourth-order nonlinear partial differential equation that describes the phase-separation behavior induced by thermal inversion. Periodic boundary conditions are employed as well as infinitesimal sinusoidal perturbations for the initial condition. The solution scheme includes local linearization (from a previous time step) through Fourier transformation, followed by the application of the Euler method to solve the resulting set of ordinary differential equations for the frequency components of the concentration. With this mathematical model, a reasonable membrane pore size profile consistent with experimental observations is obtained.

Introduction

Broens et al.[1] classified structure formation in polymer membranes into three mechanisms: (a) liquid–liquid phase separation; (b) gelation; and (c) crystallization. Liquid–liquid phase separation involves either nucleation and growth[2] or spinodal decomposition.[3] Gelation involves the formation of microcrystalline regions much smaller than the nuclei. This generally takes place at high polymer concentrations. At lower polymer concentrations (10%–20%), crystallites of sizes not much smaller than the size of the nuclei are formed. This latter type of crystallization results in the formation of lamellar or spherullitic domains.

In this work, we will only study noncrystalline systems. Thus, only liquid–liquid phase-separation processes will be considered for membrane formation. Both thermodynamics and kinetics govern this process. For the thermodynamic part of the analysis, any of a number of models such as Flory–Huggins theory,[4,5] Flory–Prigogine theory,[6–9] or even the more sophisticated thermodynamic theories of Patterson[10] and Prausnitz[11–13] can be adopted. Since we are only concerned about qualitative explanations for the formation of pore structures in polymer membranes, Flory–Huggins theory was chosen and later proven adequate for our purposes. However, for quantitative predictions, it may be more appropriate to use one of the other thermodynamic theories.

The experimental work described in part 1 of this series of papers indicates that thermal casting produces open-pore anisotropic membranes with starting compositions in the semidilute region. Such region is close to the critical composition of a binary phase diagram, where the size of the metastable region is small. This means that we need to only focus on spinodal decomposition rather than nucleation and growth as the process for phase separation.[14,15] To model spinodal decomposition, the phenomenological theory formulated by Cahn and Hilliard[16] will be used rather than other approaches involving stochastic[17–22] and molecular dynamical[23,24] formulations. Such an approach is theoretically and computationally more tractable, considering the existence of a variety of thermodynamic and transport models for polymer systems. The free-volume theory[25–28] for the mass-transport aspect of the analysis will be used in conjunction with Cahn and Hilliard's theory for the system free energy. To solve the numerical problem posed by this phase-separation analysis, we will adopt a one-dimensional version of the approach developed by de Fontaine[29] for spinodal decomposition in metal alloys. Although the method involves certain assumptions on the constitutive relations of polymeric systems, it will be shown later that the results are qualitatively correct and useful for making further predictions on the effects of other thermodynamic and kinetic parameters on the morphology of thermally cast membranes. In addition, the entire model can be easily extended to multicomponent systems and to higher dimensional cases.

Model Strategy

Before embarking on detailed modeling, we will first give a brief review of the thermal casting procedure. Thermal casting (Figure 1) induces the formation of pore structures in a polymer membrane by the removal of heat instead of by using a nonsolvent as the coagulating agent. The simplest starting material here is a binary polymer solution

* Present address: Department of Chemistry and Chemical Engineering, Michigan Technological University, Houghton, MI 49931.

0024-9297/85/2218-2545$01.50/0

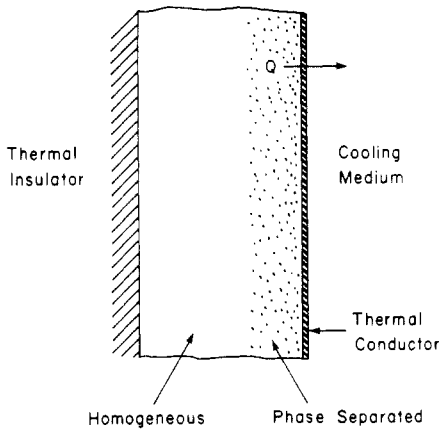

Figure 1. Schematic diagram of the formation of the structured polymer membranes through the thermal casting process. Heat is removed through the thin conducting surface, whereby phase separation is initiated, while the backside temperature is protected by the insulating substrate.

(polymer/solvent). The solution is first sandwiched between a thermal insulator and a thin thermal conductor (such as a thin metal sheet) and then heated to a temperature where the solution is homogeneous. Cooling is then suddenly applied to the thermal conductor side to initiate phase separation of the polymer solution. This temperature drop propagates from the cold face while phase separation proceeds throughout the system. When the whole membrane is phase-separated, the structure is frozen and the solvent is leached out from the phase-separated material. The result is a membrane that may or may not have varying pore size distribution along its cross section, depending on the exact casting conditions and the starting solution compositions.

To model the coagulation step (Figure 2), we divide the system into a number of thin sheets. In each of these layers, an average temperature is assumed, which changes as a function of time. Within a certain time interval, this temperature will again be averaged in time. This approach allows discretization of a continuous problem. Since our phase separation model is only one-dimensional, we also assume that the calculated concentration profiles are randomly oriented within the material layers; i.e., within each layer the material is isotropic. At a particular time after the start of the casting process, different concentration profiles are established in each of the material slices. The coagulation process is essentially completed when none of the concentration profiles change noticeably in time. Final pore size at a given material slice in the membrane is obtained from the smallest distance between polymer domains. Larger domain distances correspond to cells that are accessible only through surrounding pores. In open structures, pores occupy areas of contact amongst cells.

Model Development

Thermodynamic Equations for Phase Equilibria. Tompa[30] described the procedures to determine phase relationships for a polymer/solvent system. The polymer in the analysis is represented by a segment of the chain with the same molecular weight as the solvent. We will neglect the volume change upon mixing. For a binary system, equilibrium concentrations of coexisting phases (superscripts $'$ and $''$) must obey the following relationship

$$\mu_i' = \mu_i'' \tag{1}$$

where μ_i is the chemical potential of component i (1, solvent; 2, polymer segment). The loci of the compositions

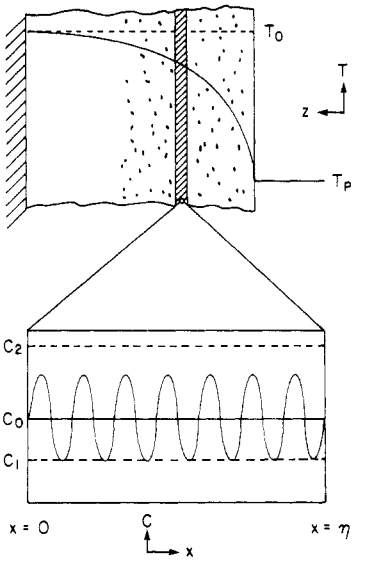

Figure 2. Model strategy for the prediction of pore size distribution for thermal-cast polymer membranes. At a given time interval, a small region along the thickness of the membrane is at a certain average temperature. Within this time interval and at the given temperature, equations for linear and nonlinear spinodal decomposition were solved to give the periodic concentration profile depicted in the enlarged view of a randomly oriented microscopic domain in the thin section.

of the phases in equilibrium (polymer-rich and solvent-rich phases) at different temperatures constitute the binodal curve. The spinodal curve can be obtained from

$$\det(\partial\mu_i/\partial x_j) = 0 \tag{2}$$

where $\partial\mu_i/\partial x_j$ is the partial derivative of the chemical potential of component i with respect to the segment fraction of component j. For a binary system, mass balance (or equivalently, segment balance) gives

$$x_1 + x_2 = 1 \tag{3}$$

We will use the polymer-segment fraction as our concentration variable, knowing that the solvent-segment fraction can be obtained from eq 3. We will also use c rather than x_2 to denote the segment fraction of polymer. Note that c is numerically equal to the weight fraction, mass fraction, mole fraction, and volume fraction of the polymer. In our formulations, we will liberally use c for any of these quantities.

Local Morphology Development. When the solution is suddenly brought to a concentration and temperature inside the spinodal curve, it will not be stable to any fluctuations however small in amplitude (Figure 3). The solution undergoes a spontaneous transformation called spinodal decomposition,[3] where the new phases are formed by a continuous flux of like molecules (segments) against the direction of concentration gradient (uphill diffusion). In contrast, regions between the binodal and spinodal curves are stable to small-amplitude fluctuations in concentration, but unstable to concentration fluctuations (called nuclei) having local compositions close to the opposite side of the binodal curve.[31] In this kind of phase transformation, called nucleation and growth, the nuclei continuously grow in size (at the expense of the outlying regions) through ordinary downhill diffusion, i.e., mass transport of phase-separating component along the direction of concentration gradient. Growth of structure by the spinodal decomposition and nucleation and growth mechanisms is illustrated in Figure 4. We note in this figure that in nucleation and growth the size of the new phase increases while the internal concentrations remain

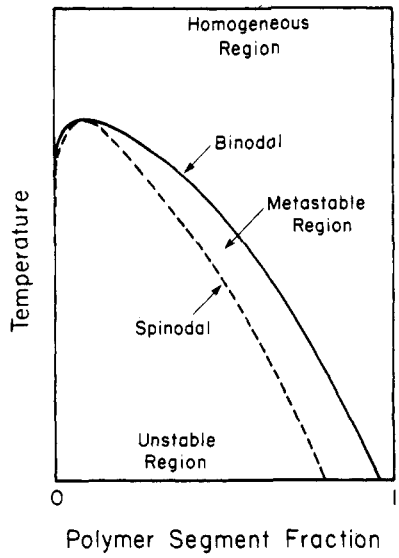

Figure 3. Regions of stability and instability in a binary polymer/solvent phase diagram. Outside the binodal curve the system is homogeneous. Inside the spinodal curve the system phase separates spontaneously into two distinct phases. In the metastable region phase separation occurs only upon the application of a finite concentration perturbation called nuclei.

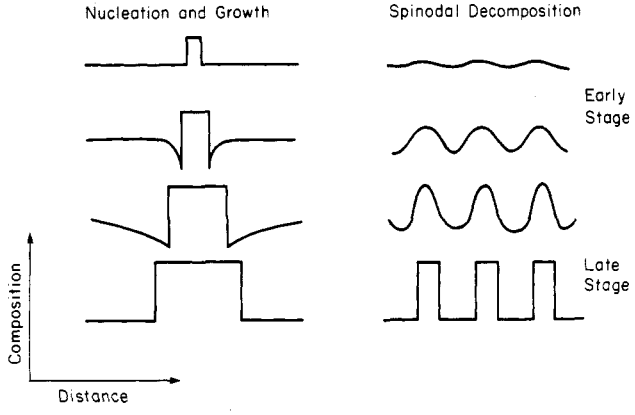

Figure 4. Schematic diagrams showing the evolution of local morphologies for two phase-separation mechanisms.

constant, whereas in growth from spinodal decomposition the size of the new phase stays roughly the same while its concentration deviation from the bulk average increases. At later stages of spinodal decomposition, the domains of the new phase increase in size by agglomeration. This ageing process, often referred to as coarsening, minimizes the surface area per unit volume of the domains of the new phase.[32]

According to Cahn,[16] the free energy (Helmholtz or Gibbs free energy) of a phase-separated system depends not only on the concentration but also on the concentration gradient. This leads to an expression for a phenomenological, coarse-grained free energy, $G(c)$, given by

$$G(c) = \int_V [f(c) + \kappa(\nabla c)^2]\, \mathbf{dr} \tag{4}$$

where $\mathbf{dr}$ corresponds to an infinitesimal volume, $f(c)$ is the local Gibbs free energy of mixing per unit volume, and κ, the so-called gradient energy coefficient, is assumed to be approximately composition-independent. This second term in the integrand accommodates contributions of the diffuse interphase between domains to the total free energy of a heterogeneous system.

To implement the chosen phenomenological theory of diffusion,[32] we define a concentration- and temperature-dependent mobility, $M(c)$, as the ratio of the diffusional flux, $\mathbf{J}$, of polymer segments to the chemical potential difference between the polymer segment and solvent:

$$\mathbf{J} = -M(c)\nabla(\mu_2 - \mu_1) \tag{5}$$

We may obtain $\mu_2 - \mu_1$ by minimizing the free-energy integral in eq 4 with respect to c, subject to the constraint

$$\int_V (c - c_0)\, \mathbf{dr} = 0 \tag{6}$$

a condition that leaves the average composition, c_0, invariant over the whole system. Thus

$$\mu_2 - \mu_1 = \partial f/\partial c - 2\kappa\nabla^2 c \tag{7}$$

To complete the derivation of the so-called diffusion equation for spinodal decomposition,[29] a differential mass balance of polymer segments within an infinitesimal control volume is invoked. Here, we will only consider diffusional contributions to the flux of material, as the system is stagnant. Thus

$$\partial c/\partial t = -\nabla\cdot\mathbf{J} \tag{8}$$

Substituting eq 5 and 7 into eq 8 gives

$$\frac{\partial c}{\partial t} = \nabla\cdot\left[M(c)\nabla\left[\left(\frac{\partial f}{\partial c}\right) - 2\kappa\nabla^2 c\right]\right] \tag{9}$$

For spinodal decomposition, we can apply a small-amplitude sinusoidal (or combinations of) perturbation in c as the initial condition. In fact, any concentration perturbation can be used as the initial condition. For the boundary conditions, the most appropriate is a periodic one, which means that in a certain spatial direction (a) the segment fraction of polymer is the same on both sides of the integration domain and (b) the amount of material entering one side of the integration domain is exactly compensated by that leaving the other side.

For the early stages of spinodal decomposition, eq 9 can be linearized along the average composition of the binary system:

$$\frac{\partial c}{\partial t} = M_0\left\{\left(\frac{\partial^2 f}{\partial c^2}\right)_0 \nabla^2 c - 2\kappa\nabla^4 c\right\} \tag{10}$$

The quantities M_0 and $(\partial^2 f/\partial c^2)_0$ are evaluated at the average composition of the system, c_0. This linearized problem has a closed-form solution[33]

$$c - c_0 = \sum_{\mathbf{K}} \exp[r(\mathbf{K})t][A(\mathbf{K})\cos(\mathbf{K}\cdot\mathbf{r}) + B(\mathbf{K})\sin(\mathbf{K}\cdot\mathbf{r})] \tag{11}$$

where $r(\mathbf{K})$, the amplification factor or growth rate, is given by

$$r(\mathbf{K}) = -[M_0(\partial^2 f/\partial c^2)_0(\mathbf{K}\cdot\mathbf{K}) + 2M_0\kappa(\mathbf{K}\cdot\mathbf{K})^2] \tag{12}$$

where $\mathbf{K}$ is the wave vector associated with the fluctuations and A and B are constants to be determined from the existing composition fluctuation in the undecomposed system. Because M_0 is always positive, $(\partial^2 f/\partial c^2)_0$ governs the sign of the growth rate. Positive values yield negative values of $r(\mathbf{K})$, causing all instabilities to decay rapidly. If the amplification factor, $r(\mathbf{K})$, is positive, the structure grows at an accelerated rate. Equation 12 allows the calculation of the resonant wavelength, λ_m, of the most rapidly growing peak in the frequency spectrum during spinodal decomposition.[33] This is done by differentiating $r(\mathbf{K})$ with respect to $\mathbf{K}$ and equating the derivative to zero. For a one-dimensional case

$$\lambda_m = 2(2^{1/2})\pi\left[-\frac{(\partial^2 f/\partial c^2)_0}{2\kappa}\right]^{-1/2} \tag{13}$$

Equations 10–13 complete the linear stability analysis, which explains the formation of structures in thermal-cast membranes nicely. However, the equations are only valid in the early stages of growth. When the system is well into the growth stage, structure formation can only be adequately gleaned by solving the nonlinear diffusion equation (eq 9).

Global Temperature Profile. The time-dependent temperature profile can be obtained from Fourier's law of heat conduction:

$$\partial T/\partial t = \alpha_T \nabla^2 T \tag{14}$$

The initial uniform temperature, T_0, corresponds to a condition in which the binary system is homogeneous, while the final temperature, T_P, lies in the region where the system phase separates. The boundary conditions are (a) at $z = 0$ and $T = T_P$ and (b) at $z = L$ and $\partial T/\partial z = 0$. For a constant thermal diffusivity, α_T, this problem has the following closed-form solution:[34]

$$\frac{T - T_0}{T_P - T_0} = 1 - \sum_{n=0}^{\infty} \frac{4(-1)^n}{(2n+1)\pi} \exp\left[-\frac{\alpha_T(2n+1)^2\pi^2 t}{4L^2}\right] \cos\left[(2n+1)\pi(L-z)/2L\right] \tag{15}$$

A constant thermal diffusivity is assumed for the determination of the global temperature profile. Specifically, we use the value for PMMA at 30 °C. This assumption is reasonable, in view of the close similarity of the solvent and polymer segment in heat conduction abilities. In addition, phase separation is assumed to entail negligible enthalpy changes. Hence, propagation of the temperature perturbation imposed on the cooling face is decoupled from the phase-separation kinetics. Equation 15, which applies to the problem of heat transfer into a finite, inert slab, is therefore justified.

Constitutive Relations. To simulate realistic polymer/solvent systems, accurate means to estimate the thermodynamic and mass-transport constitutive relations will be needed eventually. As a starting point, we aim for qualitative predictions of the formation of anisotropic structures from thermal-cast membranes. Once confirmed of their general validity, we can experimentally determine the optimal parameters for these constitutive relations to achieve quantitative predictions.

In our thermodynamic analysis, we use the Flory–Huggins theory[4] for the Gibbs free energy of mixing

$$\frac{\Delta G_m}{RT} = \frac{c}{m}\log c + (1-c)\log(1-c) + c(1-c)\chi \tag{16}$$

where m is the number of segments in a polymer chain and the Flory–Huggins interaction parameter is given by $\chi = (\alpha + \beta)/T$ (α and β are concentration and temperature independent). The parameter α accounts for the entropic contribution to χ, while β is proportional to the excess interaction energy between the polymer segment and solvent molecule. From eq 1 and 16, the governing relationship for the binodal curve becomes

$$\log(1-c') + [1-(1/m)]c' + \chi c'^2 = \log(1-c'') + [1-(1/m)]c'' + \chi c''^2$$

$$\frac{c'}{m}\log(c') - \left(1-\frac{1}{m}\right)(1-c') + \chi(1-c')^2 = \frac{c''}{m}\log(c'') - \left(1-\frac{1}{m}\right)(1-c'') + \chi(1-c'')^2 \tag{17}$$

Equations 2 and 16 give the final relationship for the spinodal curve:

$$\frac{1}{mc} + \frac{1}{1-c} - 2\chi = 0 \tag{18}$$

Note that if the sum of the terms on the left-hand side of eq 18 does not vanish, it corresponds to the thermodynamic diffusion coefficient.

Vrentas and Duda[25,26] and Huston, Cahn, and Hilliard[35] used the following mobility (or mobility factor), $M(c)$, relationship

$$M(c) = \frac{c(1-c)}{RT}[D_1^* c + D_2^*(1-c)] \tag{19}$$

where D_2^* and D_1^* are the self-diffusivities of the polymer segment and solvent molecule, respectively. Adopting the free-volume theory of Vrentas and Duda,[25-28] we have for D_1^* and D_2^*

$$D_1^* = D_{01}^* \times \exp\left[-\frac{\gamma[(1-c)\hat{V}_1^* + c\hat{V}_1^* M_{j1}/M_{j2}]}{(1-c)K_{11}(K_{21}+T-T_{G1}) + cK_{12}(K_{22}+T-T_{G2})}\right] \tag{20}$$

$$D_2^* = D_{02}^* \times \exp\left[-\frac{\gamma[(1-c)\hat{V}_1^* + c\hat{V}_1^* M_{j1}/M_{j2}]/\xi}{(1-c)K_{11}(K_{21}+T-T_{G1}) + cK_{12}(K_{22}+T-T_{G2})}\right] \tag{21}$$

Here, D_{01}^* is the front factor for D_1^*; D_{02}^*, the front factor for D_2^*, depends on the molecular weight of the polymer and the ratio of the number of segments (with entanglement effects) to the number of freely orienting segments; ξ is the ratio of the critical molar volume of the solvent jumping unit to the critical molar volume of the polymer jumping unit; $\hat{V}_1^*$ is the specific critical hole free volume of the solvent required for a jump; M_{ji} is the molecular weight of the jumping unit of component i; K_{11} and K_{12} are free-volume parameters for the solvent; K_{21} and K_{22} are free-volume parameters for the polymer; γ, an overlap factor for free volume, is introduced because the same free volume is shared by more than one molecule; and, T_{Gi} is the glass-transition temperature of component i. All these parameters are assumed to be independent of concentration and temperature. Finally, the mutual diffusion coefficient is given by the product of the mobility and the thermodynamic diffusion coefficient.

For the gradient energy parameter, κ, Debye's thermodynamic theory of nonhomogeneous solutions[36] yields

$$\kappa = RT\chi l^2/6 \tag{22}$$

where l is the range of molecular interactions between the polymer and solvent. A typical range of 50–300 Å is often cited.[14] In our analysis, we assign a value of 300 Å for l and consider it to be independent of temperature and composition.

Numerical Solution of the Nonlinear Diffusion Equation

Solution of the nonlinear diffusion equation for structural growth from spinodal decomposition is difficult even in one dimension. To solve this problem in real space, a domain length should be chosen in such a way as to encompass several peaks in the concentration profile. The reason is that the periodic boundary condition imposed is quite unnatural; peaks close to the edges are affected by edge effects. Hence, a minimum number of peaks must be covered to remove numerical artifacts. With this minimum number of peaks, many grid points are needed for the PDE problem. This is compounded by the stiffness problem encountered especially during the accelerated

growth stage of phase separation. We find it necessary to be able to move grid points to regions where large changes in the concentration gradient occur. With the PDE problem that has a fourth-order spatial derivative, errors can be quickly magnified, creating immense stability problems for the entire numerical scheme. Satisfactory solution procedure has yet to emerge. Even if a feasible numerical scheme for the direct solution of this PDE problem is found, it will probably incur massive amounts of digital computing time. We will thus adopt a numerical approach similar to that used by de Fontaine[29] in the solution of an analogous PDE problem for spinodal decomposition in metal alloys. Specifically, the PDE is solved in the Fourier or reciprocal space. The dependent variable becomes a set of frequency components (or amplitudes) for the polymer segment fraction, and the independent variable becomes a set of wavenumbers (or frequencies). This approach reduces the PDE problem to the solution of a set of ODEs for a finite number of frequency components. Time-dependent polymer segment fraction profiles are subsequently constructed via inverse Fourier transformation.

The above solution scheme requires much less computing time than any possible real-space solution. In fact, the problem can now be solved even in three dimensions, although with much more computing time than a solution in one dimension. Even though this method directly yields frequency spectra, such a result is as useful as concentration profiles because we are only interested in interdomain distances. The only disadvantage of this method is that it requires finite-ordered polynomial approximations for the concentration-dependent mutual diffusivity and mobility, thus restricting the choices of material and transport property relations. As shown by de Fontaine,[29] this restriction is not crucial for metal alloys because parabolic curves are adequate for the mutual diffusivity and mobility of these systems. For polymer solutions, we have to take these quantities up to the third order, as they are known to be strong functions of concentration and temperature.[25-28] In the following discussion, we will sketch the essentials of this numerical scheme.

We start by redefining the dependent variable as

$$u = c - c_0 \tag{23}$$

This definition is made only for convenience. Equation 9 is still to be solved in its entirety, only this time we replace c by u. To convert the integration domain to the reciprocal space, we multiply eq 9 by $(1/V)\exp(-i\beta\cdot\mathbf{r})\,d\mathbf{r}$ and integrate over the domain V

$$\frac{1}{V}\int_V \frac{\partial u}{\partial t}\exp(-i\beta\cdot\mathbf{r})\,d\mathbf{r} = \frac{1}{V}\int_V \nabla\cdot[M(u)\nabla\Phi]\exp(-i\beta\cdot\mathbf{r})\,d\mathbf{r} \tag{24}$$

where

$$\Phi = \partial f/\partial u - 2\kappa\nabla^2 u \tag{25}$$

A first application of Greens Theorem to the right-hand side of eq 24 (see Appendix A) yields

$$\frac{1}{V}\int_V \nabla\cdot[M(u)\nabla\Phi]\exp(-i\beta\cdot\mathbf{r})\,d\mathbf{r} = -\frac{i\beta}{V}\int_V M(u)\nabla\Phi\exp(-i\beta\cdot\mathbf{r})\,d\mathbf{r} \tag{26}$$

The surface integral vanishes because of the periodic boundary conditions. For the left-hand side of eq 24, we use Leibnitz Rule (see Appendix B) to obtain

$$\int_V \frac{\partial u}{\partial t}\exp(-i\beta\cdot\mathbf{r})\,d\mathbf{r} = \frac{d}{dt}\int_V u\exp(-i\beta\cdot\mathbf{r})\,d\mathbf{r} \tag{27}$$

Again, the surface integral vanishes because of the periodic boundary conditions. The mobility, $M(u)$, and mutual diffusivity, $D(u)$, are given by the cubic approximations

$$M(u) = M_0 + M_1u + M_2u^2 + M_3u^3$$
$$D(u) = D_0 + D_1u + D_2u^2 + D_3u^3 \tag{28}$$

where M_i and D_i are temperature-dependent quantities. Substituting D and M (eq 28) into eq 24 and applying the Greens Theorem and Leibnitz Rule (eq 26 and 27, respectively), we obtain

$$\frac{1}{V}\frac{d}{dt}\int_V u\exp(-i\beta\cdot\mathbf{r})\,d\mathbf{r} = \frac{i\beta}{V}\int_V (D_0 + D_1u + D_2u^2 + D_3u^3)\nabla u\exp(-i\beta\cdot\mathbf{r})\,d\mathbf{r} - \frac{2\kappa i\beta}{V}\int_V (M_0 + M_1u + M_2u^2 + M_3u^3)\nabla^3 u\exp(-i\beta\cdot\mathbf{r})\,d\mathbf{r} \tag{29}$$

In order to use the Fourier transform method which tolerates only linear terms, we must, at this stage, use a linearization process that is somewhat arbitrary. This is done in the following manner. Let us assume that at some time t_0 a solution $u_0 = u(\mathbf{r},t_0)$ is known (the initial condition, for example). Within a short time interval Δt, we may write u_0 for u in the expression for D and M in eq 29. Next, in order to eliminate the space dependence of the terms for D and M, we expand the known solution u_0 in a Fourier series

$$u_0(\mathbf{r}) = \sum_{\mathbf{K}'} C^0_{\mathbf{K}'}\exp[i\beta'\cdot\mathbf{r}] \tag{30}$$

$$u_0^2(\mathbf{r}) = \sum_{\mathbf{K}'}\sum_{\mathbf{K}''} C^0_{\mathbf{K}'}C^0_{\mathbf{K}''}\exp[i(\beta' + \beta'')\cdot\mathbf{r}] \tag{31}$$

$$u_0^3(\mathbf{r}) = \sum_{\mathbf{k}'}\sum_{\mathbf{K}''}\sum_{\mathbf{K}'''} C^0_{\mathbf{K}'}C^0_{\mathbf{K}''}C^0_{\mathbf{K}'''}\exp[i(\beta' + \beta'' + \beta''')\cdot\mathbf{r}] \tag{32}$$

where the C^0's are complex amplitudes corresponding to the Fourier transforms of u_0. Equations 30–32 are then back-substituted into eq 29, and the Greens Theorem is employed the required number of times to reduce the derivative terms in u. This procedure is carried out with the constraint of vanishing surface integrals due to the periodic boundary conditions. After grouping terms, we obtain the final expression

$$\frac{dC_{\mathbf{K}}}{dt} = -\beta^2[D_0 + 2\kappa M_0\beta^2]C_{\mathbf{K}} - \beta\sum_{\mathbf{K}'}(\beta - \beta')C^0_{\mathbf{K}'}[D_1 + 2\kappa M_1(\beta - \beta')^2]C_{\mathbf{K}-\mathbf{K}'} - \beta\sum_{\mathbf{k}'}\sum_{\mathbf{K}''}(\beta - \beta' - \beta'')C^0_{\mathbf{K}'}C^0_{\mathbf{K}''}[D_2 + 2\kappa M_2(\beta - \beta' - \beta'')^2]C_{\mathbf{K}-\mathbf{K}'-\mathbf{K}''} - \beta\sum_{\mathbf{K}'}\sum_{\mathbf{K}''}\sum_{\mathbf{K}'''}(\beta - \beta' - \beta'' - \beta''')C^0_{\mathbf{K}'}C^0_{\mathbf{K}''}C^0_{\mathbf{K}'''}[D_3 + 2\kappa M_3(\beta - \beta' - \beta'' - \beta''')^2]C_{\mathbf{K}-\mathbf{K}'-\mathbf{K}''-\mathbf{K}'''} \tag{33}$$

where all summations are from $-\infty$ and ∞. Note that this formulation is still in three dimensions because the $\mathbf{K}$'s represent an ordered triplet of wavenumber indexes.

We can now reduce the problem to a one-dimensional case by the substitution

$$\mathbf{r} \rightarrow x$$
$$\mathbf{K} \rightarrow k \qquad (k = -\infty, ..., -2, -1, 0, +1, +2, ..., +\infty) \tag{34a}$$

If 2λ denotes the length of the domain, a Fourier component of wave index k corresponds to a wavenumber

$$\beta_k = k\pi/\lambda \tag{34b}$$

and a wavelength

$$\lambda_k = 2\pi/k \tag{35}$$

For convenience, we define

$$\alpha_k{}^{i} = -\beta_k(D_i + 2\kappa M_i\beta_k{}^2) \tag{36}$$

In actual computation, it is advantageous to use only positive integers for k, up to as large a value as time permits. From the definition of the Fourier transforms, negative indexes are eliminated by

$$C_{-k} = C_k{}^* \qquad C_0 = 0 + i0 \tag{37}$$

with the asterisk denoting the complex conjugate. With these conditions, we obtain an Euler-type algorithm for the solution of the frequency components, C_k, of wavelengths, λ_k, as functions of the wave index, k,

$$C_k = C^0{}_k + \Delta t\beta_k[(\alpha_k{}^\circ + \alpha_k{}^2\tilde{C}_0 + \alpha_k{}^3\bar{\tilde{C}}_0) - (\alpha_k{}^1C^0{}_{2k} + \alpha_k{}^2\tilde{C}_{2k} + \alpha_k{}^3\bar{\tilde{C}}_{2k})C^0{}_k{}^* + \sum_{\substack{h=0\\h\neq k}}^{n}[(\alpha_h{}^1C^0{}_{k-h} + \alpha_h{}^2\tilde{C}_{k-h} + \alpha_h{}^3\bar{\tilde{C}}_{k-h})C^{0*}{}_k - (\alpha_h{}^1C^0{}_{k+h} + \alpha_h{}^2\tilde{C}_{k+h} + \alpha_h{}^3\bar{\tilde{C}}_{k+h})C^{0*}{}_h]] \quad (k = 1, 2, ..., n) \tag{38}$$

with

$$\tilde{C}_j = \sum_{i=1}^{n}(C^0{}_iC^0{}_{j-i} + C^{0*}{}_iC^0{}_{j+i} + C^0{}_iC^0{}_{i-j}) \tag{39}$$

and

$$\bar{\tilde{C}}_j = \sum_{i=1}^{n}\sum_{q=1}^{n}[C^0{}_iC^0{}_qC^0{}_{j-i-q} + C^0{}_iC^0{}_qC^{0*}{}_{i+q-j} + 2(C^0{}_iC^0{}_qC^0{}_{j-i+q} + C^0{}_iC^0{}_qC^0{}_{i-q-j})] \tag{40}$$

In eq 39 and 40, j must range from 1 to $3n$ to ensure that all relevant terms in the summations are included.

Equations 38–40 enable us to compute explicitly the n unknown amplitudes C_k at time $t = t_0 + \Delta t$ as functions of the known $C^0{}_k$ at time t_0. This operation may be repeated to step up in time. At any stage, the concentration profile may be easily constructed by the inverse Fourier transform

$$u(x,t) = 2\sum_{k=1}^{n}(A_k\cos\beta_kx - B_k\sin\beta_kx) \tag{41}$$

where

$$C_k = A_k + iB_k \tag{42}$$

Equations 38–42 lead to a useful parameter, p, the percent completion, defined by

$$p = 100(\sigma/\sigma_0) \tag{43}$$

where

$$\sigma_0 = (c_0 - c_1)(c_2 - c_0) \tag{44}$$

c_1 and c_2 being the equilibrium compositions. Also, from Parseval's relation[29] and eq 41

$$\sigma^2 = 2\sum_{k=1}^{n}(A_k{}^2 + B_k{}^2) \tag{45}$$

To ascertain convergence of the above numerical scheme, different time steps are taken until there is negligible change in the results. Also, we use a frequency range that includes subharmonic peaks with nonvanishing frequency components. Many frequency points are used to outline secondary peaks in the frequency range of the main harmonics. With this approach, stability has been more readily achieved than with any direct procedures in the real space. This is probably due to fact that the Fourier transform technique, which makes use of repeated integrations, is more stable than methods that use repeated differentiations (such as finite difference, finite element, and collocation methods).[29] In spite of the approximations employed for the constitutive relations, this method is capable of revealing qualitative features of phase-separation behaviors, such as spinodal decomposition, growth from nucleation, and even phase coarsening.

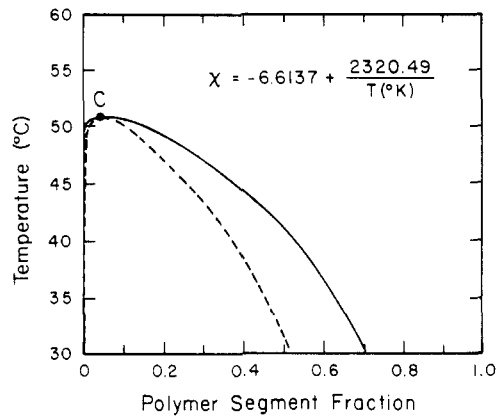

Figure 5. Binary phase diagram obtained from the Flory–Huggins theory with a concentration-independent χ-parameter. Functional dependence of the χ-parameter is shown in the inset.

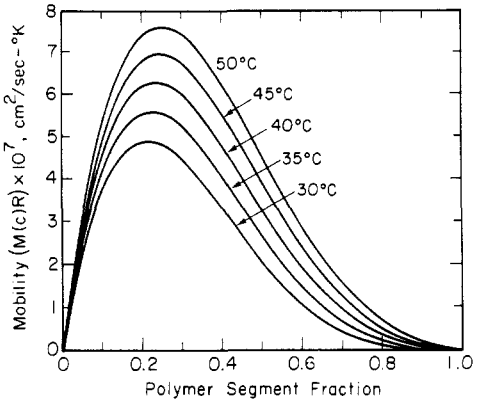

Figure 6. Dependence of the mobility factor on temperature and concentration calculated by using the free-volume parameters listed in Table I.

Results and Discussion

In order to discuss our simulation results systematically, we first pick a reference case. This corresponds to thermal inversion of a 0.1 polymer segment fraction solution, initially at 80 °C, and suddenly brought down to 30 °C at the cold face. The experimental binodal composition data reported in part 1 of this series of publications can be sufficiently fitted with the Flory–Huggins theory that has a concentration-independent χ-parameter given by $-6.6137 + 2320.49/T(\mathrm{K})$. Figure 5 shows the calculated binodal and spinodal curves for this χ-relation using eq 17 and 18. Note that the critical point, C, is at 51 °C and at a polymer segment fraction of 0.045.

The mobility factor as functions of composition and temperature (Figure 6) is obtained with the local mass-transport parameters listed in Table I. The mobility increases with temperature, since the free volume increases as well. At a given temperature, the mobility exhibits a relative maximum with composition, whose location de-

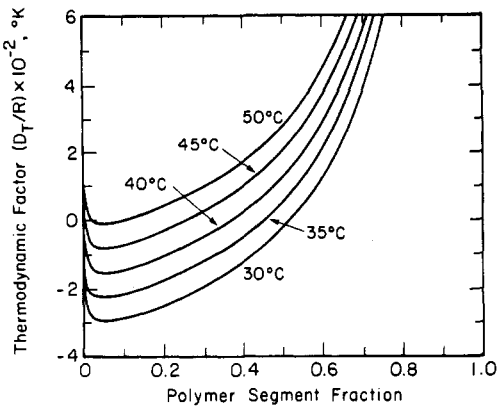

Figure 7. Dependence of the thermodynamic factor on temperature and concentration calculated by using the Flory–Huggins theory with the χ-parameter function shown in Figure 5.

Table I
Transport Parameters for the Model System

$D_{01}^* = 1 \times 10^{-3}$ cm^2/s	$K_{22}/T_{G2} = 0.2116$
$K_{21}/T_{G1} = 0.2667$	$D_{02}^* = 1 \times 10^{-2}$ cm^2/s
$K_{11}T_{G1}/\gamma\hat{V}_1^* = 4$	$K_{12}T_{G2}/\gamma\hat{V}_1^* = 4$
$M_{j1}/M_{j2} = 1$	$\xi = 0.5$

pends on the relative values of the self-diffusivities of the polymer segment and solvent molecule. Since our chosen set of transport parameters (Table I) assumes that the self-diffisuvities for the polymer segment are generally greater than those for the solvent molecule, maxima in our mobility vs. concentration curves are located at polymer segment fractions less than 0.5. (See also eq 19.) Note that the mobility vanishes for the pure components. This does not necessarily cause any problem for the mutual diffusion coefficient, as the thermodynamic factor (Figure 7) goes to infinity for the pure components. The thermodynamic factor is negative for concentrations inside the spinodal curve. When its value is 0, the corresponding concentration coincides with that of the spinodal. Note also that the absolute magnitude of the thermodynamic factor decreases with increasing temperature. The product of the mobility factor in Figure 6 and the thermodynamic factor in Figure 7 gives the mutual diffusivity as functions of temperature and concentration (Figure 8). For concentrations inside the spinodal, the diffusivity follows the same trend as that for the thermodynamic factor; i.e., it is negative, with its absolute magnitude decreasing with increasing temperature. For concentrations outside the spinodal, the diffusivity follows the same trend as that for the mobility; i.e., it is positive, with its absolute magnitude increasing with temperature. Such complex behavior has a strong influence on the predicted morphology, as will be discussed below.

Cubic polynomial approximations of the mobility and mutual diffusivity are derived by imposing the following conditions for mobility, M: (1) $M^a(c = 0) = M(c = 0) = 0$; (2) $(c^*)^a = c^*$; (3) $M^a(c^*) = M(c^*)$; and (4) $M^a(c^{**}) = 0$. Superscript a denotes the approximate values. The quantity, c^*, is the value of c where M is a maximum, and c^{**} is the value of c where M^a exhibits a relative minimum ($M^a(c)$, a cubic approximation of $M(c)$, has a relative maximum and minimum with c). Conditions 1 and 4 ensure that the approximate mobility function never assumes a negative value, while conditions 2 and 3 match the maximum point, which often falls within the confines of the unstable region. For the mutual diffusivity, D, (1) $(c_1)^a = c_1$; (2) $D^a(c^\dagger) = D(c^\dagger)$; (3) $(c^{\dagger\dagger})^a = c^{\dagger\dagger}$; and (4) $D^a(c'') = D(c'') = 0$. Again, superscript a denotes the approximate values, $c^\dagger$ is the value of c where D is a relative minimum,

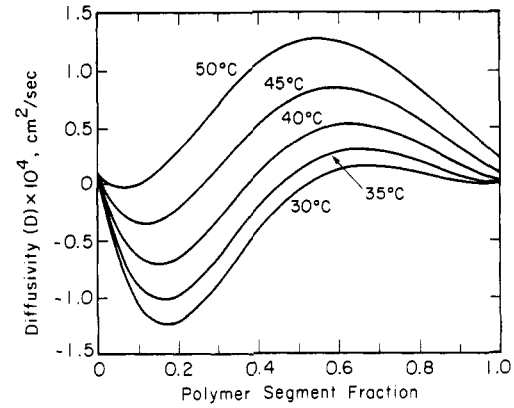

Figure 8. Dependence of the mutual diffusivity on temperature and concentration as obtained from the thermodynamic and transport parameters used in Figures 5–7.

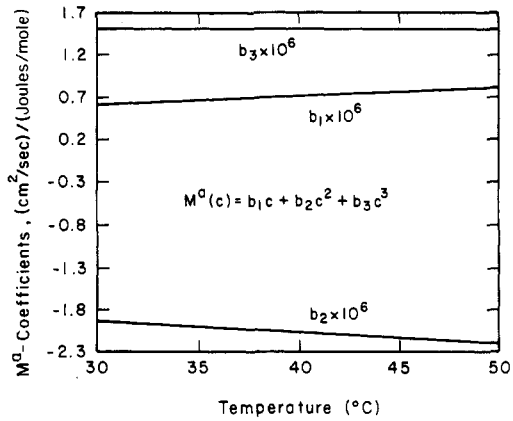

Figure 9. Fitted values of the cubic coefficients for the mobility factor as functions of temperature.

$c^{\dagger\dagger}$ is the value of c where D is a relative maximum (for homogeneous polymer solutions, i.e., for concentrations outside the binodal curve, $D(c)$ usually has a relative maximum), c_1 is the solvent-rich binodal composition, and c'' is the polymer-rich spinodal composition. Conditions 1 and 4 ensure a certain degree of thermodynamic consistency in the approximate mobility and mutual diffusivity functions. Although condition 3 does not assure us of the same binodal compositions for the true and approximate functions, we will show later that it helps to enforce condition 4. Lastly, condition 2 is employed to achieve more or less the same minimum value for the mutual diffusivity inside the spinodal region. With these assumptions, we satisfactorily approximate the true functions for the mobility and diffusivity inside the spinodal region. In addition, the approximate functions predict the exact solvent-rich binodal compositions. However, the predicted polymer-rich binodal compositions are closer to, if not exactly coincident with, the spinodal compositions. The calculated temperature-dependent cubic coefficients for $M^a(c)$ and $D^a(c)$ are shown in Figures 9 and 10. Figures 11 and 12 compare the cubic approximations for the mobility and diffusivity with those calculated from the free-volume theory. Note that at this temperature the approximate functions fit the true functions well for compositions inside the spinodal. Since the cubic approximations for the mutual diffusivity cross the abscissa in three locations, the application of condition 4 for the mutual diffusivity ensures that the approximate diffusivity does not cross the abscissa inside the spinodal region.

Figures 13–17 show the evolution of structure in a system after a sudden drop in temperature. Here, the system

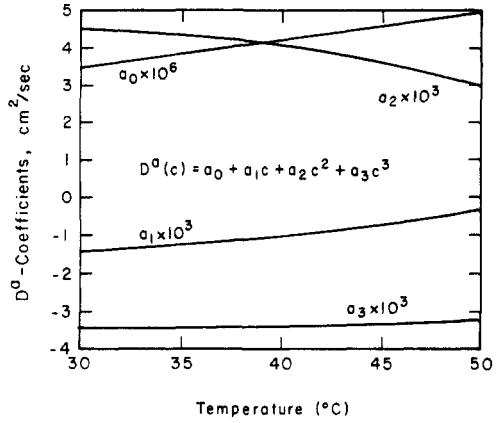

Figure 10. Fitted values of the cubic coefficients for the mutual diffusivity as functions of temperature.

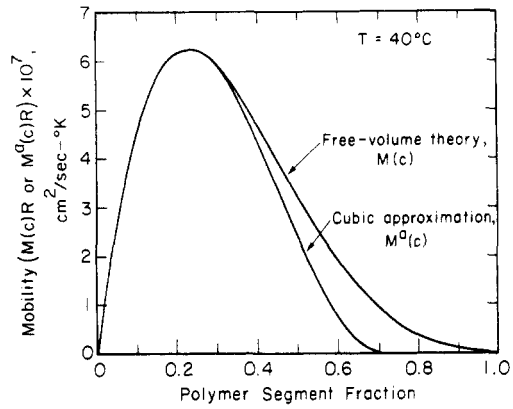

Figure 11. Comparison of mobilities calculated by the free-volume theory and its cubic approximation. At 40 °C, the range of polymer segment fraction of interest is 0–0.37, where the two curves are close to each other.

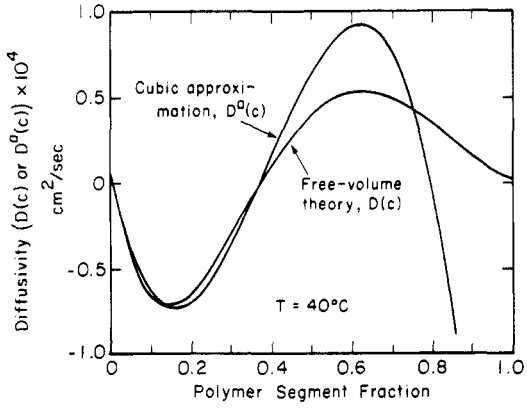

Figure 12. Comparison of mutual diffusivities obtained from the free-volume theory and its cubic approximation. At 40 °C, the range of polymer segment fraction of interest is 0–0.37, where the two curves are close to each other.

is initially homogeneous at a temperature above the spinodal temperature. The system temperature is then abruptly reduced to 30 °C where phase separation occurs. In our experimental system, this case is typical for the portion of the polymer solution that is adjacent to the cooling medium. Thus, the calculated final periodicity of about 0.18 μm can be taken as the pore size of that layer in the membrane. This value is remarkably close to the periodicity of 0.16 μm obtained from linear spinodal decomposition theory (eq 13). In all the cases we have thus far investigated, the final pore size is a little bigger than what is predicted from the linear theory. The pattern for the deviation, as typically shown in Figure 13, is a gradual

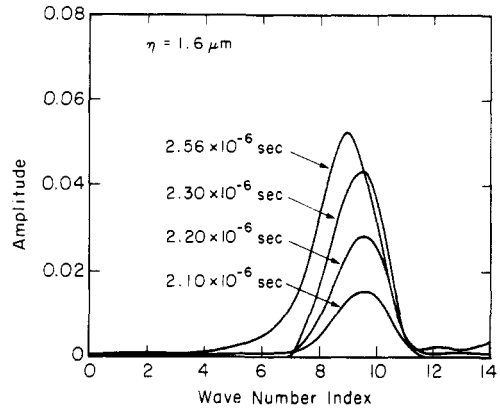

Figure 13. Frequency spectra for the evolution of structure in a model system quenched from a temperature above the spinodal to 30 °C. At this temperature, the system phase separates, and peaks for domain periodicities are shown at different lapsed times. Values of domain periodicities are equal to η divided by wavenumber indexes.

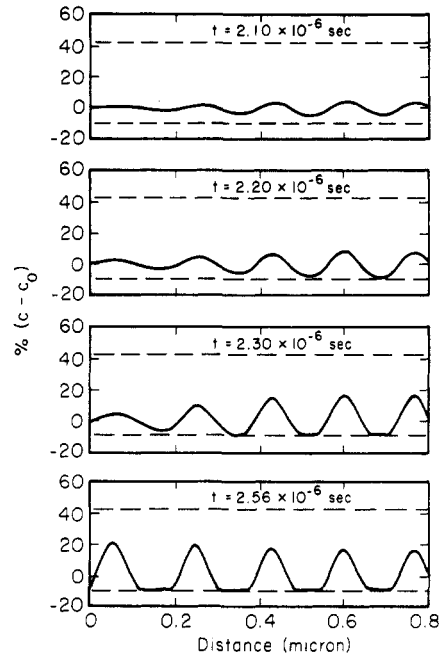

Figure 14. Polymer segment profiles as functions of time during the evolution of structure for the system described in Figure 13. Dashed lines are binodal compositions obtained from the cubic approximations. Only the left half of the profiles are plotted to clearly show domain profiles as well as periodicities.

shift of the main peak to the low-frequency end of the spectrum. From Figure 14, however, this deviation is insignificant. Thus, linear spinodal decomposition theory can adequately predict final pore sizes for structural growth from a step drop in temperature. Figure 15 reveals three stages in the evolution of structure for a phase-separated system. At the start of phase separation, the system adjusts from its initial composition perturbation. Perturbations at frequencies other than resonance dissipate in favor of a periodicity consistent with linear spinodal decomposition theory. Growth of structure in this induction period (which extends to about 10% completion) is very slow compared to that in the next stage. In the second stage of growth, the structure evolves at an accelerated rate. The percent completion vs. time curve is very steep, and movement in the concentration profiles is apparently in the vertical direction. After this growth stage, the structure continues to evolve at a much slower rate. This ripening stage includes the coarsening process which in-

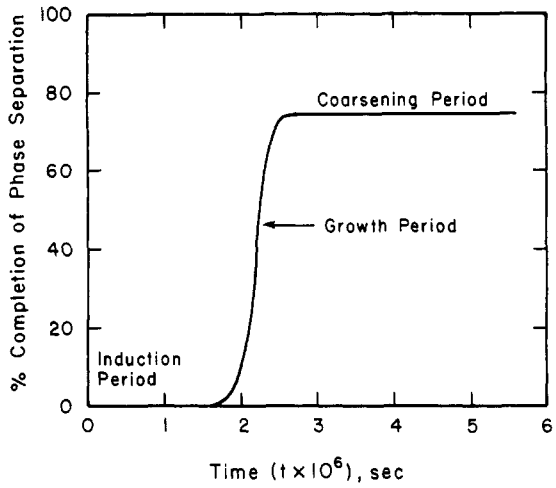

Figure 15. Extent of phase separation for the system described in Figure 13 showing three regions of structure evolution: induction, accelerated growth, and ripening or phase-coarsening stages.

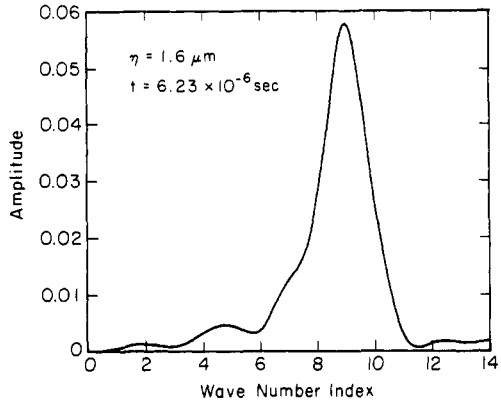

Figure 16. Frequency spectrum for the system described in Figure 13 in its coarsening stage. Here, the main peak is preserved along with some outgrowth in the low-frequency end.

volves the dissolution of some of the phase domains and the growth in size of others.[29] As shown in Figure 16, coarsening preserves the main peak that was formed in the growth stage. The dissolution of some of the polymer domains (Figure 17) is reflected by the outgrowth of low-frequency components in Figure 16.

To determine the effects of the continuous lowering of temperature during spinodal decomposition in membranes, we solve the diffusion equation at 40 °C, and then at certain points in its structure evolution (at about 0.6% and 8.7% completion) the system temperature is again lowered to 30 °C. The same final pore size of 0.25 μm (as the system that is coagulated at 40 °C all the way) is obtained for the latter case. For the former case, we obtained a final pore size of 0.22 μm. This series of simulation work indicates that once the structure is about 5% complete the periodicity no longer changes, even if the system temperature is reduced. However, if the system temperature continues to drop while the phase-separation process is still in its infancy, the final pore size can be easily altered. For other cases, this critical percent-completion value may be higher. The same average concentration value at 5% completion for 40 °C is equivalent to a higher percent-completion value at a higher temperature because σ_0 (eq 44) decreases with increasing temperature. Thus, the cut-off number of 40% completion proposed by de Fontaine[29] may be quite reasonable. For the determination of pore sizes of membrane filters and separators, the evolution of low-frequency structures during the coarsening stage is not

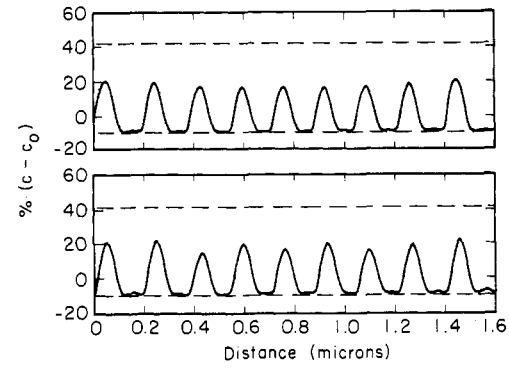

Figure 17. Comparison of polymer segment profiles for the system described in Figure 13 at the end of the growth stage and at the beginning of the coarsening stage. During coarsening (bottom plot), continued growth of some of the polymer domains is accomplished through the dissolution of the others. Again, the dashed lines correspond to binodal compositions obtained from cubic approximations for the mobility and diffusivity.

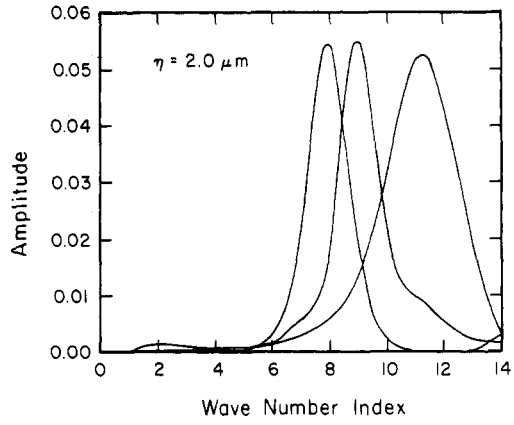

Figure 18. Frequency spectra at the end of the growth stages (at around 80% completion) for systems with different thermal histories. For the left and center peaks, the system temperature is first dropped to 40 °C and later to 30 °C. After the first temperature drop, the system is allowed to achieve percent-completion values of 8.7 and 0.6. The temperature is then lowered to 30 °C. For the former case, frequency locking occurs; i.e., the same spectrum (left peak in the figure) was finally obtained as that for a system that is maintained at 40 °C. For the latter case, the middle spectrum was obtained. The right spectrum was obtained for a single temperature drop to 30 °C.

very significant because their open-pore structures correspond to honeycombed cells that are bounded by smaller open pores. Thus, any computation beyong 40% completion would be a waste of time and effort. Figure 18 summarizes the above discussion by three curves, corresponding to a straight drop to 30 °C and a case where the sample is first lowered to 40 °C then to 30 °C.

The above numerical procedure and parameter values are applied to simulate the formation of a 300-μm thermal-cast membrane. The diffusion equation is solved at six locations along the thickness of the membrane (z = 0, 4, 10, 75, 200, and 300 μm). Temperature histories of material at these locations are obtained from eq 15. Figure 19 gives the predicted pore size profile for the thermal-cast membrane. Here, the pore size adjacent to the cooling medium is about 0.18 μm, while the pore size adjacent to the thermal insulator is about 1.33 μm. This resulting pore size distribution is a clear manifestation of the possibility of obtaining anisotropic membranes from the thermal coagulation of binary solutions. In addition, this modeling work can be used to explain effects of casting conditions in the pore distribution of product membranes. Finally, certain conclusions that are applicable to the formation

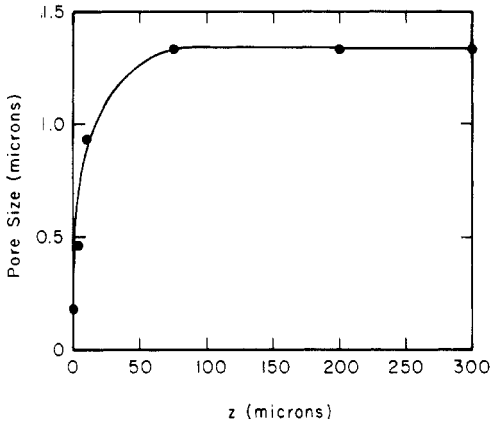

Figure 19. Pore size distribution for a 300-μm thermal-cast membrane. The pore size at the cold side is about 0.18 μm, while the pore size at the thermal insulator side is about 1.2 μm. Solid curve joins circled computer simulation data points.

of phase-inversion membranes can be derived from this work.

The existence of an accelerated growth stage in structure formation and the adequacy of linear spinodal decomposition theory in pore size predictions can greatly simplify the analysis of pore size distribution for the formation of thermally cast membranes. In a given slice of material in the polymer membrane, the temperature is continuously dropping. However, due to the very brief acceleration period, structural growth for a particular slice of material virtually occurs at only one temperature. In this membrane problem where the temperature in a given material slice is continuously dropping, we observed that the induction period before the growth stage is approximately the same as that for the case where the material slice is subjected to a single temperature drop (at the growth temperature). Therefore, the analysis of the membrane-formation process reduces to the determination of induction periods for different quenching temperatures. Figure 20 shows that the induction period increases with temperature. It takes more time for structure to develop at a higher quenching temperature because the initiation period is longer. Note that with linear spinodal decomposition (eq 13), Flory–Huggins (eq 16), and Debye (eq 22) theories, we derive that the pore size for sudden temperature drops increases with increasing coagulation temperature. Thus, larger pores can be obtained if the material is given enough time to phase separate at a temperature close to the spinodal temperature. Smaller pores can be obtained with less amount of phase-separation time at lower temperatures.

Conclusion

Formation of anisotropic structures in thermal-cast polymer membranes can therefore be explained through spinodal decomposition. We have also shown that coarsening preserves the relevant polymer-domain periodicities established in the growth stage of spinodal decomposition. Even though our numerical approach involves certain approximations in the constitutive relations, we think that our results are qualitatively correct and adequate for its future applications to other phase-separating systems. These other systems include ternary polymer solutions, polymer blocks and blends, and nonpolymeric phase-separated systems.

In our analysis of linear and nonlinear spinodal decomposition theories, we concluded that for our model case the linear theory can adequately predict relevant pore sizes of thermal-cast membranes. Changes in domain periodicities during the growth stage are negligible, and only low-frequency components of the pore size evolution spectrum are affected by coarsening. The cutoff pore size which corresponds to the peak with highest frequency is therefore roughly the same as what was predicted from the linear theory. From the solution of the nonlinear theory for a step drop in temperature (from a value where the system is homogeneous to that where it phase separates), we observed that the growth period is relatively short compared with induction and coarsening times. In addition, we found that the induction period increases with the phase-separation temperature. Finally, we obtained an anisotropic pore size distribution for a thermal-cast membrane with a detailed simulation of the formation process.

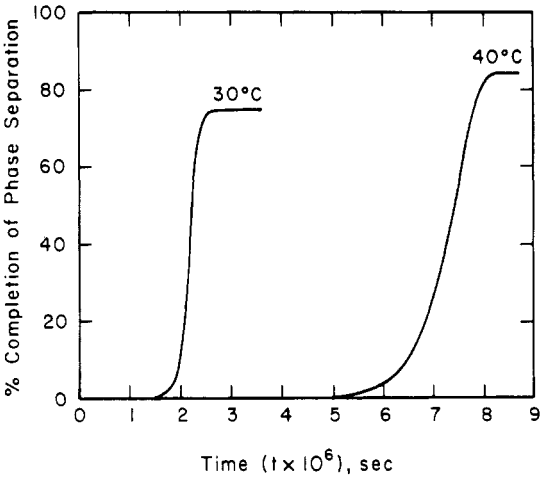

Figure 20. Percent-completion curves for single step drops in temperature. The induction period for 30 °C is less than that for 40 °C. Coarsening starts at higher percent-completion values at 40 °C than at 30 °C. This is due to the higher value of σ_0, the average equilibrium polymer segment fraction deviation at 30 °C.

Acknowledgment. This work was supported by the Polymer–Polymer Composites Program of the Center for Advanced Materials of Lawrence Berkeley Laboratory and the National Science Foundation through Grant CPE-8318681.

Appendixes

A. Greens Theorem. The volume integral

$$\int_V \psi \nabla(M \nabla \theta)\, d\mathbf{r}$$

can be transformed into another volume integral plus a surface integral by applying the Greens Theorem:[29]

$$\int_V \psi \nabla(M \nabla \theta)\, d\mathbf{r} = -\int_V \nabla\theta(M \nabla \psi)\, d\mathbf{r} + \int_S M\psi(\partial\theta/\partial n)\, d\mathbf{S} \quad \text{(A1)}$$

In the last integral, $\partial\theta/\partial n$ denotes the partial derivative of θ along the outward normal to the surface S which bounds the volume V. If the functions θ and ψ obey the periodic boundary conditions, the surface integral vanishes. In our case

$$\psi = \exp(-i\beta \cdot \mathbf{r}) \quad \text{(A2)}$$

and

$$\theta = u \text{ or } \partial f/\partial u - 2\kappa\nabla^2 u \quad \text{(A3)}$$

Thus, with the following periodic boundary conditions

$$\theta(\mathbf{s}) = \theta(-\mathbf{s})$$

$$\partial\theta(\mathbf{s})/\partial n = -\partial\theta(-\mathbf{s})/\partial n \quad \text{(A4)}$$

(s being the value of r on the surface S) the surface integral in eq A1 vanishes.

B. Leibnitz Rule. The quantity

$$\int_V (\partial u/\partial t) \exp(-i\beta\cdot\mathbf{r})\, d\mathbf{r}$$

can be transformed into

$$\frac{d}{dt}\int_V u \exp(-i\beta\cdot\mathbf{r})\, d\mathbf{r} - \int_S u\mathbf{V}_s \exp(-i\beta\cdot\mathbf{r})\, d\mathbf{S}$$

by the application of the Leibnitz rule.[37] In the second integral, $\mathbf{V}_s$ denotes the normal velocity of the surface. With the above-mentioned periodic boundary conditions (eq A4), the surface integral vanishes.

References and Notes

(1) Broens, L.; Altena, F. W.; Smolders, C. A.; Koenhen, D. M. *Desalination* **1980**, *32*, 33.
(2) Volmer, M.; Weber, A. *Z. Phys. Chem.* **1925**, *119*, 277.
(3) Cahn, J. W. *Acta Metall.* **1961**, *9*, 795.
(4) Flory, P. J. *J. Chem. Phys.* **1942**, *10*, 51.
(5) Huggins, M. L., presented before the Wilder D. Bancroft Colloid Symposium, Ithaca, New York, June 20, 1941.
(6) Flory, P. J. Fifteenth Spiers Memorial Lecture, *Trans. Faraday Soc.* **1970**.
(7) Flory, P. J.; Eichinger, B. E. *Trans. Faraday Soc.* **1968**, *64*, 2035.
(8) Flory, P. J.; Hoeker, H. *Trans. Faraday Soc.* **1971**, *67*, 2258.
(9) Prigogine, I.; Bellemans, A.; Mathot, V. "The Molecular Theory of Solutions"; North Holland: Amsterdam, 1957; Chapter 16.
(10) Patterson, D. *Macromolecules* **1969**, *2*, 672.
(11) Heil, J. F.; Prausnitz, J. M. *AIChE J.* **1969**, *12*, 678.
(12) Bonner, D. C.; Prausnitz, J. M. *AIChE J.* **1973**, *19*, 943.
(13) Renuncio, J. A. R.; Prausnitz, J. M. *Macromolecules* **1976**, *9*, 898.
(14) McMaster, L. P. "Aspects of Liquid–Liquid Phase Transition Phenomena in Multicomponent Polymeric Systems"; Platzer, N. B., Ed.; American Chemical Society: Washington, DC, 1975; Adv. Chem. Ser., No. 142, pp 43–65.
(15) Nishi, T.; Wang, T. T., Kwei, T. K. *Macromolecules* **1975**, *8*, 227.
(16) Cahn, J. W.; Hilliard, J. E. *J. Chem. Phys.* **1958**, *28*, 258.
(17) Rao, M.; Kalos, M. H.; Lebowitz, J. L.; Marro, J. *Phys. Rev. B: Solid State* **1976**, *13*, 4328.
(18) Bortz, A. B.; Kalos, M. H.; Lebowitz, J. L.; Zendejas, M. A. *Phys. Rev. B: Solid State* **1974**, *10*, 535.
(19) Levy, A.; Reich, S.; Meakin, P. *Phys. Lett. A* **1982**, *87A*, 248.
(20) Sanji, P. S.; Gunton, J. D.; Katz, S. L.; Timpe, R. H. *Phys. Rev. B: Condens. Matter* **1982**, *25*, 389.
(21) Kock, S. W.; Desai, R.; Abraham, F. F. *Phys. Rev. A* **1982**, *26*, 1015.
(22) Haus, J. W.; King, H. *Phys. Rev. B: Condens. Matter* **1982**, *2*, 3298.
(23) Abraham, F. F.; Schreiber, D. E.; Mruzik, M. R.; Pound, G. M. *Phys. Rev. Lett.* **1976**, *36*, 261.
(24) Mruzik, M. R.; Abraham, F. F.; Pound, G. M. *J. Chem. Phys.* **1978**, *69*, 3462.
(25) Vrentas, J. S.; Duda, J. L. *J. Polym. Sci., Polym. Phys. Ed.* **1977**, *15*, 403.
(26) Vrentas, J. S.; Duda, J. L. *J. Polym. Sci., Polym. Phys. Ed.* **1977**, *15*, 417.
(27) Vrentas, J. S.; Duda, J. L. *Macromolecules* **1976**, *9*, 785.
(28) Vrentas, J. S.; Duda, J. L.; Ni, L. W. *Macromolecules* **1983**, *16*, 261.
(29) de Fontaine, D. Ph.D. Dissertation, Northwestern University, Evanston, IL, 1967.
(30) Tompa, H. "Polymer Solutions"; Butterworths: London, 1956.
(31) Smolders, C. A.; van Aartsen, J. J.; Steenbergen, A. *Kolloid Z. Z. Polym.* **1971**, *243*, 14.
(32) de Fontaine, D. "Thermodynamics and Kinetics of Phase Separation, Metallurgical Treatises"; Tien, J. K.; Elliott, J. F., Ed.; American Institute of Metallurgical Engineers: Warrendale, PA, 1981; pp 423–444.
(33) Feke, G. T.; Prins, W. *Macromolecules* **1974**, *7*, 527.
(34) Carslaw, H. S.; Jaeger, J. C. "Conduction of Heat in Solids", 2nd ed.; Oxford at the Clarendon Press: London, 1959.
(35) Huston, E. L.; Cahn, J. W.; Hilliard, J. E. *Acta Metall.* **1966**, *14*, 1053.
(36) Debye, P. *J. Chem. Phys.* **1959**, *34*, 680.
(37) Reddy, J. N.; Rasmussen, M. L. "Advanced Engineering Analysis"; Wiley: New York, 1982.

Preliminary Study of the Kinetics of Phase Separation in High Molecular Weight Poly(methyl methacrylate)/Solution-Chlorinated Polyethylene Blends

R. G. Hill, P. E. Tomlins,* and J. S. Higgins

Department of Chemical Engineering and Chemical Technology, Imperial College of Science and Technology, London SW7 2BY, England.

Received February 13, 1985

ABSTRACT: Preliminary results of a study of the kinetics of spinodal decomposition in a high molecular weight blend of poly(methyl methacrylate) with solution-chlorinated polyethylene using small-angle light, X-ray, and neutron scattering are reported. The data are compared with the theoretical predictions of Cahn, Hilliard, and van Aartsen. The phase separation occurs initally on a scale much smaller than previously observed for polymeric systems.

Introduction

Despite an ever increasing interest in the thermodynamics of polymer miscibility, there have been comparatively few studies of the kinetics of phase separation in polymer mixtures.

Several theories exist (Pincus,[1] de Gennes,[2] Binder[3]) that describe the process of phase separation in high molecular weight polymer blends where the molecular weights of the components are above their entanglement values. These theories, although differing in their approaches, predict the wavelength of the dominant concentration fluctuation (λ_m) to be of the same order of magnitude as the radius of gyration (R_g) of the polymer for deep quenches. In contrast van Aartsen,[4] using Cahn–Hilliard[5–7] and Flory–Huggins[8,9] theory, predicts that this wavelength will be much larger than R_g and lie in the micron range. λ_m is defined by van Aartsen as

$$\lambda_m = 2\pi l\left[3\left(\frac{T}{T_s} - 1\right)\right]^{-1/2} \quad (1)$$

where l is the Debye[10] range of molecular interaction and T_s and T are the temperature of the spinodal and sample, respectively. This equation differs from the one given by

0024-9297/85/2218-2555$01.50/0